NUMERICAL INVESTIGATION OF HEAT TRANSFER IN SPIRALLY COILED CORRUGATED PIPES: ASSESSMENT OF TURBULENCE MODELS

***Milan ĐORĐEVIĆ*[*1], *Marko MANČIĆ*[2], *Velimir STEFANOVIĆ*[2], *Mića VUKIĆ*[2]**

[*1]Faculty of Technical Sciences, University in Priština - Kosovska Mitrovica, Serbia

[2]Faculty of Mechanical Engineering, University of Niš, Serbia

[*] Corresponding author; E-mail: milan.djordjevic@pr.ac.rs

The Archimedean spiral coil made of a transversely corrugated pipe represents the radiant heat absorber of a parabolic dish solar concentrator. The main advantage of the considered design is the coupling of two passive methods for heat transfer enhancement - coiling the flow channel and changing the surface roughness. The aim of this numerical study is to assess the capability of Reynolds-averaged Navier-Stokes models of different complexity (Realizable k-ε, SST k-ω and RSM Linear Pressure-Strain) to adequately represent the heat transfer phenomena in the considered complex flow geometry for wide ranges of Reynolds and Prandtl numbers.

The obtained results indicate that the Realizable k-ε model with enhanced wall treatment is inadequate to simulate the heat transfer for all flow conditions, while both SST and RSM slightly overestimate experimental data in the turbulent region and are able to predict laminarisation at low Reynolds numbers. The SST model predictions are more accurate in the transitional and at the beginning of the turbulent region, irrespective of the curvature ratio. RSM predictions are generally more accurate in the turbulent region. Numericaly obtained circumferential distributions of local Nu number reveal that considered turbulence models are unable to completely anticipate the interactions between the complex flow in the basic section of the pipe and the vortex flow within the corrugations.

Key words: *Corrugated Spiral Coil, Heat Transfer, Numerical Simulation, Turbulence modeling*

1. Introduction

Modern paraboloidal concentrators require compact and efficient heat absorbers to convert solar radiation into heat energy. This research is directed towards a design solution that involves the development of the heat absorber made of spirally coiled pipe with transverse circular corrugations.

The main advantage of the considered design is the coupling effect of two passive methods for heat transfer enhancement - coiling the flow channel and changing the surface roughness. The presence of the superimposed secondary flow in curved channel flow suppresses axial propagation of initial turbulent fluctuations, so that the transition from laminar to turbulent flow is delayed [1, 2]. The spiral coil flow is characterized by two critical Reynolds numbers, the first one when the turbulence has set only in the outer turns with lowest curvature ratio, and the second one, when the inertia forces,

even in the innermost turns with highest curvature ratio, are sufficient to overcome the damping effect of the secondary flow. Accordingly, all three flow regimes (laminar, transitional and turbulent) could occur in the spiral coil at the same time.

In contrast to the flow stabilizing effect of curvature, transversal corrugations act as turbulence promoters, since the turbulence level is increased by the separation and reattachment mechanism. Furthermore, Morton [3] found that heated pipes also develop vortices resulting from a combination of radial-directional and downward motions of fluid particles induced by displacement of boundary layer.

Systematic numerical studies on the applicability of different turbulence models for flow in curved channels and over corrugated surfaces could be rarely found in the literature. Several numerical studies that examined the laminar flow and heat transfer phenomena in smooth spiral channels have been published. Numerical investigations of turbulent flow conditions in smooth spiral-coil pipes are less frequent in literature compared to the previous ones. They used the Standard k-ε turbulence model [4, 5], RNG k-ε with standard wall functions [6] and Linear Pressure-Strain RSM [7] to simulate the flow and heat transfer characteristics. Eulerian two-phase turbulent model was utilized to simulate nanofluid flow and heat transfer in the spirally coiled tube with and without helical ribs [8].

Even though the interest in spiral coiled systems is on the rise, they are less popular compared to helical tubes, which have attracted major attention in the study of coiled tubes for heat transfer. Some of these papers investigate laminar flow of Newtonian fluids in coils with corrugated and dimpled walls [9-11]. Realizable k-ε model is the most commonly used for numerical investigations on thermal performance of helical coils with helical [12, 13] and spherical [14] corrugations and the multi-head twisted tube structure [15]. Improved k-ω model was used for evaluation of the heat transfer in a corrugated coil tube with lobe-shaped cross section and twisted tapes as swirl generators [16]. The only study found in the literature evaluating the adequacy of different turbulence models for predicting heat transfer in a smooth coil with constant curvature used the Standard k-ε model with wall functions, the SST k-ω model and the second-order RSM [17]. The tested SST model showed the best agreement with the experimental data.

Previous experimental investigations [18, 19] clearly indicate the dominant effects affecting the thermal-hydraulic processes in the spirally coiled corrugated tube exposed to radiant heating: the simultaneous development of the flow due to the continuously changing curvature along the length of the spiral coil, the existance of complex secondary flow caused by the superposition of inertial and buoyant force, separation and reattachment of the boundary layer over corugations and the occurrence of recirculating vortex flow within the corrugations, as well as the nonuniformity of the boundary conditions, both in the axial direction and around the circumference of the tube. Conducted numerical experiments led to the conclusion that an exact assessment of the overall impact of the mentioned effects on heat transfer is virtually impossible only by consistent application of theoretically selected turbulence models without the existence of relevant empirical data for their evaluation and calibration.

To the best of authors' knowledge, this is the first systematic attempt to evaluate the usability of the turbulence models based on the Reynolds-averaged Navier-Stokes (RANS) equations for the calculation of thermal-hydraulic processes in a coiled pipe with constantly changing curvature and structured roughness elements at the wall. The main goal of this study is the synthesis of realistic numerical formulations that are consistent with the complex nature of secondary flows, as well as the assessment of the ability of three-dimensional numerical models to predict single-phase flow and heat transfer in curved pipes with transverse corrugations.

2. Geometric and numerical models

The Archimedean spiral, with a pitch slightly larger than the maximal outside diameter of the corrugated coiling pipe, was selected out of different types of spirals in order to achieve the most favorable ratio of active surface area and the total volume of the heat absorber in the parabolic dish receiver. The geometric parameters of the commercially available transversely corrugated pipe [20] and transversely corrugated Archimedean spiral coil are shown in Tab. 1.

Table 1. Geometric parameters of tested configurations

Transversely corrugated straight pipe [20]				Transversely corrugated Archimedean spiral coil			
d	9.3	mm	minimum internal diameter	R_{min}	25	mm	minimum radius of the coil
d_0	11.7	mm	maximum internal diameter	R_{max}	202	mm	maximum radius of the coil
d_{max}	12.2	mm	maximum external diameter	n	13	-	number of coil turns
s	0.25	mm	wall thickness	L	9.324	m	length of the coil
e	1.2	mm	corrugation depth	p_s	13.6	mm	spiral coil pitch
p_c	4.2	mm	corrugation pitch				

Due to the limitations of computer resources and complexity of the real object's geometry, the three-dimensional numerical domain does not contain the entire spiral, but only its smaller characteristic segments, whose lengths are equal to the length of the eleven corrugation pitches. These segments are characterized by different values of curvature ratio δ and represent the geometric parameters of each of the thirteen spiral turns. Curvature ratio is defined as $\delta = d/2R$, where d is minimum internal diameter of corrugated pipe and R is radius of curvature of the coil. In case of constantly changing curvature, it is more appropriate to use the average curvature ratio $\delta_{ave} = d/2R_{ave}$, where R_{ave} is the averige radius of each spiral coil turn. For this particular case, average curvature ratio varies from 0.024 (corresponding to the 1st or outermost spiral turn) to 0.146 (corresponding to the 13th or innermost spiral turn). For illustration, the geometric models of the 5th and 12th spiral turn are shown in Figs 1 and 2, respectively.

In addition to the segments of the corrugated spiral, each of the considered geometric models contains an inlet and an outlet section. The inlet sections are smooth pipes with an inside diameter equal to the minimum inside diameter of the corrugated segment and have the same radii of curvature. The curve angles of all inlet sections are greather than 270 degrees (except for case of the smallest spiral turn), which guarantees the developed flow profiles at the inlets of corrugated segments for the considered flow conditions. The outlet sections are relatively short straight pipe segments that are added to correctly define the boundary conditions at the outlets of the corrugated numerical domains, and to prevent error propagation from the outlet boundary within the numerical domain of interest. The function of the inlet section is to provide a hydrodynamically developed flow at the inlet of the corrugated pipe, while the outlet section provides the flow without disturbances at the outlet of the corrugated pipe.

The lengths of the pipe segments used for the numerical simulations are small compared to the real absorber model. This simplification is possible because the sinusoidal profiles of the corrugations are repeated in the direction of the primary flow. The velocity field changes depend on the repetitive geometric structure of the corrugated pipe, but the existence of a hydrodynamically fully developed

flow can be assumed if the repetitive velocity profiles are identical. On the other hand, the temperature changes along the axial coordinate, but the temperature distribution pattern can be considered the same along relatively short sections. Thus, the numerical analysis can be simplified by representing the geometric domain with a larger number of smaller segments that represent the characteristic geometry.

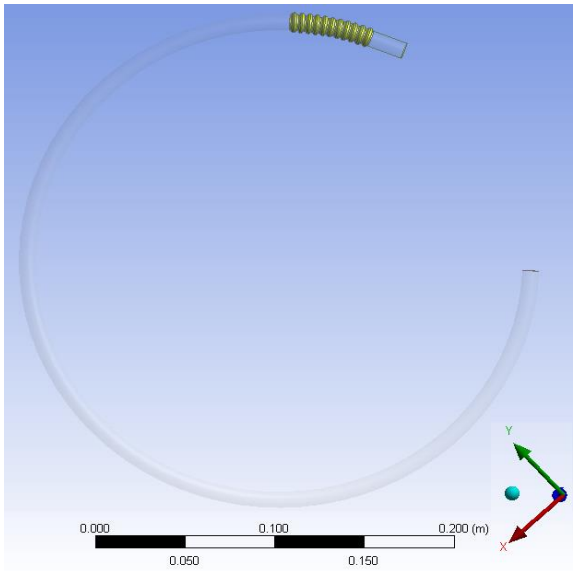

Figure 1. Geometric model of the 5th turn of spiral coil (δ_{ave}=0.033)

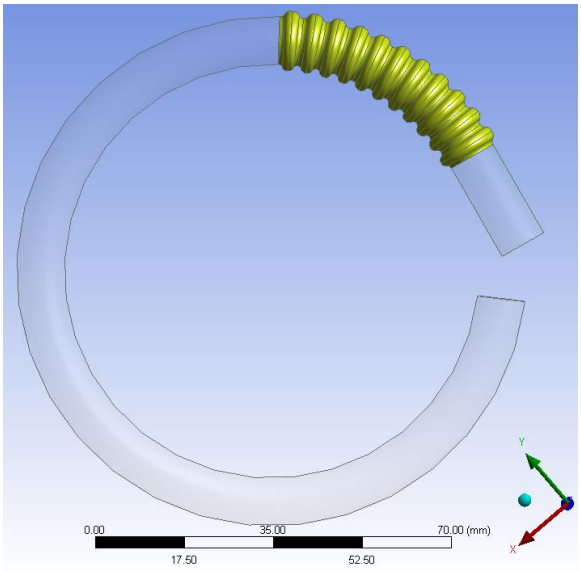

Figure 2. Geometric model of the 12th turn of spiral coil (δ_{ave}=0.102)

This numerical study has been carried out after getting a detailed insight into the necessary theoretical background and previous research works, as well as after analyzing the experimental results and determining the thermo-hydraulic characteristics of the spirally coiled corrugated pipe exposed to radiant heat [2, 18, 19]. The experimental data help to evaluate the performance of three Ansys Fluent (version 15) turbulence models based on the RANS equations. The two-equation models (Realizable k-ε and SST k-ω model) and the second-order Reynolds Stress Model (RSM, Low-Re Modifications to the Linear Pressure-Strain Model) were tested. Realizable k-ε is the contemporary model with substantial improvements over the standard k-ε model where the flow features include strong streamline curvature, vortices, flow separation and complex secondary flow features [21]. The Shear-Stress Transport (SST) k-ω model was developed to effectively blend the robust and accurate formulation of the k-ω model in the near-wall region with the freestream independence of the k-ε model in the far field. This feature makes the SST k-ω model more accurate and reliable for a wider class of flows, especially for adverse pressure gradient flows (flow separation) [21]. The RSM is the most elaborate type of RANS turbulence model in Fluent. Abandoning the isotropic eddy-viscosity hypothesis, the RSM closes the RANS equations by solving transport equations for the Reynolds stresses, together with an equation for the turbulent dissipation rate ε [21]. Since the RSM accounts for the effects of streamline curvature, swirl, rotation, and rapid changes in strain rate in a more rigorous manner than two-equation models, it has greater potential to give accurate predictions for complex flows. However, the fidelity of RSM predictions is still limited by the closure assumptions employed to model various terms in the exact Reynolds stresses transport equations [21].

Using the finite volume method, the following set of the conservation equations are formulated in the Cartesian coordinate system in the tensor form ($i, j \in \{1, 2, 3\}$):

- the continuity equation

$$\frac{\partial}{\partial x_{\mathrm{i}}}\left(\rho u_{\mathrm{i}}\right)=0 \tag{1}$$

- the momentum equations

$$\frac{\partial}{\partial x_{\mathrm{j}}}\left(\rho u_{\mathrm{i}} u_{\mathrm{j}}\right)=\rho g_{\mathrm{i}}-\frac{\partial p}{\partial x_{\mathrm{i}}}+\frac{\partial}{\partial x_{\mathrm{j}}}\left[\mu\left(\frac{\partial u_{\mathrm{i}}}{\partial x_{\mathrm{j}}}+\frac{\partial u_{\mathrm{j}}}{\partial x_{\mathrm{i}}}-\frac{2}{3}\delta_{\mathrm{ij}}\frac{\partial u_{\mathrm{l}}}{\partial x_{\mathrm{l}}}\right)\right]+\frac{\partial}{\partial x_{\mathrm{j}}}\left(-\rho\overline{u'_{\mathrm{i}}\,u'_{\mathrm{j}}}\right) \tag{2}$$

where u and u' represent velocity components and fluctuation velocity components, respectively. The energy equation is formulated separately for each of the considered turbulence models in Ansys Fluent and will be omitted here for the sake of brevity. Exact formulations of the models and the values of the constants could be found in the literature [21].

The use of wall functions (semi-empirical modeling of the velocity field near the wall) is not recommended in cases where the effects of relatively low Re numbers are present in the flow domain (within the corrugations in this case), as well as in the presence of a pronounced influence of body forces (centrifugal and buoyant forces in this case). Standard wall functions are not applicable for precise determination of the heat transfer in cases where the boundary layer separates [22], as is the case in this study. Although *k-ε* models are not designed for the near-wall flow, the adequacy of the Realizable *k-ε* model was tested by simulating the near-wall effects with the enhanced wall treatment.

Thermophysical properties of water [23, 24] and a mixture of propylene glycol and water (90% and 10% by volume, respectively) [24, 25] were treated as temperature-dependent and obtained as polynomial functions of temperature, which is crucial for an adequate interpretation of flow and heat transfer at high values of wall heat flux.

2.1. Grid generation

Selected turbulence models were formulated to explicitly resolve the viscous sublayer, which makes them independent of empirical relations determined for specific and different flow conditions. This requires a very fine mesh near the wall, where the centroids of cells adjacent to the wall need to be at a dimensionless wall distance $y^{+}\leq 1$. It is important to note that the precise value of the friction velocity U_{τ} (as well as the y^{+}) is only known *a posteriori*, because it depends on the flow itself. Therefore, a good practical assessment of the resulting flow is necessary, and when performing the final spatial discretization, it is recommended to use adaptive methods offered within the software package itself.

ANSYS ICEM CFD was used for generating a nonuniform hybrid mesh. The region near the wall was discretized with a very fine structured mesh consisting of prismatic cells. The rest of the domain was discretized with unstructured tetrahedral mesh, not only to reduce computational requirements, but also due to the fact that the discretization software failed to create a structured numerical mesh of adequate quality in the complex geometry considered. It should be noted that the mesh generation process within the complex domain is the most critical part of the entire simulation process from the point of needed computational resources.

Dimensions of the first cell layer adjacent to the wall are determined so that the centroids of these cells are located at the dimensionless wall distance $y^+ \leq 1$ for all studied cases. The viscous sublayer was discretized with 15 cell layers and the wall-normal expansion ratio 1.15 in the radial direction. Details of the entire geometry of the studied problem are incorporated into the generated hybrid numerical grid. For illustration, the details of one of the generated grids are shown in Figs 3 and 4 (Re≈3,650; Pr = 5.5 and δ_{ave}=0.033).

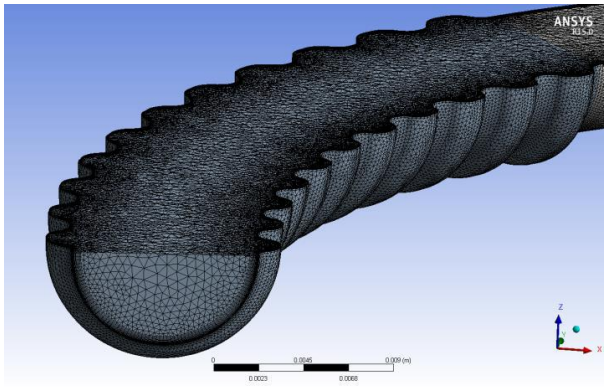

Figure 3. Display of generated numerical grid

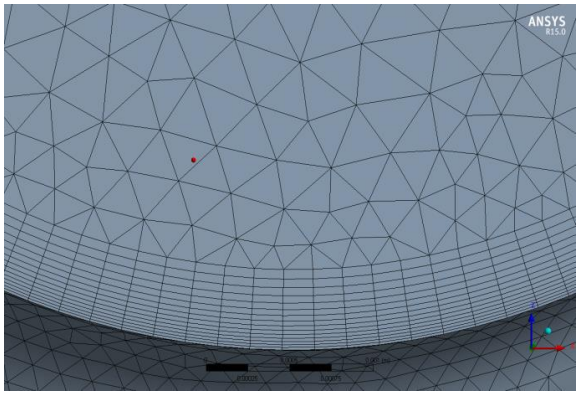

Figure 4. An enlarged view of the near-wall grid resolution

A careful check for the grid-independence of the numerical solutions has been made to ensure the accuracy and validity of the numerical scheme. Numerical calculations indicated that the value of curvature ratio δ is the most critical for the validation of turbulence models, because the largest differences between numerical results and experimental data [18] were obtained for the highest curvature. On the other hand, the assessment of the numerical grid quality on the accuracy of the solution was performed for the case with the maximum experimental value of the Re number (Re=16,800; Pr=6.7) [18].

The corrugated segment outlet bulk temperature and the peripherally averaged Nu number on the 9th corrugation of the 12th coil turn (δ_{ave}=0.102, Fig. 2) have been used to test the independency of the calculation results from the applied grids (results are reported in Tab. 2). The calculations have been carried out using the RSM (low Re number modifications to the linear pressure-strain model) on four different grids and the relative errors of the control variables were calculated.

Different grids were obtained by varying the number of structured layers in near-wall region (10-20 layers), the expansion ratio value (1.1-1.2) and the maximum size of the cells within the rest of the numerical domain (in all cases $y^+ \leq 1$). The considered numbers of cells refer only to the corrugated segment and do not include cells within the inlet and outlet segments.

Initial and boundary conditions for the grid-independence tests were formulated as follows: V_{in}=1.62 ms^{-1}, T_{in}=22°C, q_{wall}=9,492 Wm^{-2}, $(u, v, w)_{ini}$=0 ms^{-1} and T_{ini}=22°C. As the incident radiation is not uniform in the focal plane of the parabolic dish solar concentrator, the heat flux upon the tube external surfaces will vary not only in the circumferential direction, but also in the axial direction. The incident heat flux distribution on outside surfaces of corrugated segments was obtained by detailed 3-D numerical procedure using S2S Hemicube method [26]. The applied numerical model of radiation was previously precisely calibrated according to the experimental data. Obtained profiles of the flux density of absorbed radiation were imported directly into the flow simulations as wall boundary

conditions. This procedure guarantees the physical validity and accuracy of the wall boundary conditions without imposing assumptions and approximations. The validity of numerically obtained boundary conditions was verified by comparing numerical and analytical results for flat surfaces, while grid-independence tests guarantee their accuracy [26].

Table 2. Relative errors of the outlet bulk temperature and peripherally averaged Nu number (δ_{ave}=0.102; Re=16,800; Pr=6.71)

	Number of cells			
	(I)	(II)	(III)	(IV)
	936,999	1,371,249	2,185,081	2,979,657
Outlet bulk temperature [°C]	22.24	22.22	22.18	22.17
Relative error of outlet temperature [%]	0.34	0.23	0.05	-
Periph. averaged Nu number on 12^{th} turn [-]	313.8	310.2	308.3	307.4
Relative error of Nu number [%]	2.1	0.9	0.3	-

Thermal boundary conditions at the surface of the corrugated segment that is not exposed to thermal radiation were defined using the convective criterion for the considered experimental conditions. Adiabatic boundary conditions are defined at the surfaces of the inlet and outlet sections. Heat conduction trough the wall was modeled using "Shell conduction" approach [21]. The material of the wall is stainless still AISI 304.

Asymptotic convergence of control variables with increasing number of cells is evident. The Nu number predictions are more sensitive to grid quality compared to the outlet temperature. The obtained differences between grids I and II are the effect of the increase in the number of layers within the viscous sublayer, while the differences between grids II and III are due to the increase in the number of cells in the rest of the numerical domain. It can be concluded that grid resolution higher than $2.1 \cdot 10^6$ cells (case III, the second finest grid) in the studied geometry would be sufficient to produce physically realistic results independent from the applied numerical grid even for the highest Re number simulated. The corrugated segment consists of a total of 11 corrugations, which means that more than $1.9 \cdot 10^5$ cells need to be generated per single corrugation. Selected grid is characterized by a geometric refinement imposed on the wall, with 15 layers of cells and the wall-normal expansion ratio of 1.15 in the radial direction.

2.2. Description of numerical approach

The transport equations were discretized by the finite volume method and solved using the "Pressure-based solver". The Semi-Implicit Method for Pressure-Linked Equations (SIMPLE) algorithm was employed to introduce pressure into the continuity equation.

In the presence of relatively large body forces (centrifugal and buoyant forces) and strong vorticity, it is necessary to form a very fine numerical grid in regions with high pressure gradient. This can be avoided by using an alternative inperpolation "Body-force-weighted" scheme based on the estimation (weighting) of the body forces. Despite the discretization of the numerical domain with a very fine mesh, this pressure interpolation method was accepted in the study due to the dominant influence of body forces and the existence of complex secondary flows.

The discretization of a convective term in transport equations was carried out using the second-order upwind scheme. The second-order scheme was applied because implicit formulation, despite good stability, can cause numerical errors known as "false diffusion". For laminar flow cases, the "Power law" scheme for momentum discretization was used to accelerate the convergence of the solution, while pressure interpolation was performed by the "PRESTO!" scheme, since it is more accurate than the others for flow in curved channels [21]. The discretization and treatment of the continuity equation is an inherent choice of the software. The linearized set of equations was solved using the point implicit (Gauss-Seidel) solver in tandem with the algebraic multigrid (AMG) method. The convergence is achieved with values not higher than 10^{-4} for all variables and 10^{-6} for temperature.

The convergence of the iterative procedure is accelerated with increasing Re number, while increasing curvature ratio δ demonstrates the opposite effect. The intensity of the heat flux at the wall has no significant effect on the rate of convergence and the stability of the procedures. Between 600 and 1,000 iterations are required to meet the given convergence criteria for the turbulent flow cases considered, while approximately twice as many iterations are required in the laminar flow cases. Computer system used for numerical calculations was Dell Precision T5600 Workstation with two Intel Xeon E5-2667 processors and 32 GB of RAM. Comptaional time varied from less than one hour to several hours and primarily depends on the applied turbulence model and flow conditions.

3. Results and discussion

Predictions of the peripherally averaged local Nu number, as well as circumferential distribution of Nu number, were compared with experimental results [18] in order to assess the ability of the tested RANS turbulence models to adequately represent heat transfer in the considered complex flow geometry.

Peripherally averaged local Nu numbers have been calculated on the 9^{th} corrugation of spiral coil segments (Figs 1 and 2) by tested RANS turbulence models. The ability of turbulence models to predict laminarization and their accuracy in the transitional flow regime were also tested.

Predictions of turbulence model was evaluated by varying the Re and Pr numbers and the curvature ratio δ. Figure 5 shows the graphic comparisons of the tested turbulence models predictions (Realizable k-ε, SST k-ω and RSM Linear Pressure-Strain) with the correlated experimental values of peripherally averaged Nu numbers throughout the whole Re number test range for the curvature ratio values δ_{ave}=0.033 (5^{th} coil turn) and δ_{ave}=0.102 (12^{th} coil turn). Those two curvature ratio values were chosen to make the data comparable.

All applied turbulence models overestimate the values of peripherally averaged Nu numbers in general, except the RSM in the transitional flow in the case of lower value of the curvature ratio δ. The use of the Realizable k-ε model is inadequate for predicting heat transfer for all considered values of Re number and curvature ratio δ, regardless of the fact that no wall functions have been used, so that the predictions of this model will not be considered further.

The predictions of the applied SST and RSM models are relatively well-matched with the experimental data in the turbulent flow regime. Both models predict a uniform transition between the laminar and turbulent regimes, which is not in agreement with the experimental data. Predictions of both models significantly overestimate the experimentally obtained values in the laminar flow regime.

This should be especially taken into account for the conditions when different flow regimes (laminar, transitional and turbulent) can appear simultaneously in the spiral coil.

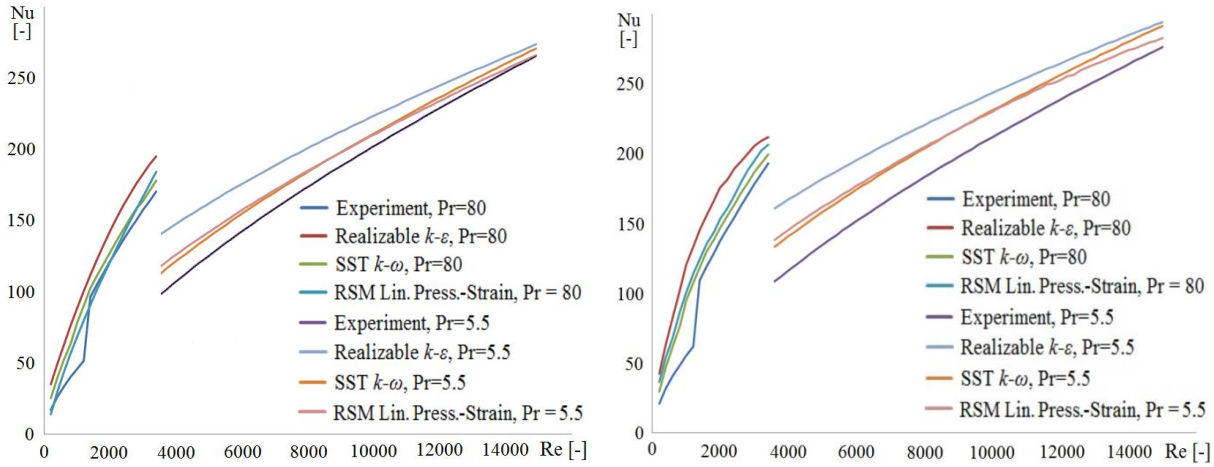

Figure 5. Comparison of the predictions of different turbulence models with experimental values of peripherally averaged Nusselt numbers for δ_{ave}=0.033 (left) and δ_{ave}=0.102 (right)

It should be noted that, irrespective of the value of the curvature ratio δ, the SST model predictions are more accurate in the transitional region and at the beginning of the turbulent region. In general, RSM predictions are more accurate in the turbulent region, especially at the end of the considered range of Re number. Predictions of both models are comparable and closely matched, no significant differences can be observed, although there are differences in value trends.

Characteristic of all flow regimes is that the differences between the experimental values of peripherally averaged Nusselt numbers and predictions of numerical models increase with increasing curvature ratio δ, whereas in the turbulent regime these differences decrease with increasing Re number.

Since the experimentally obtained data for peripherally averaged Nusselt number have an oscillatory character in the turbulent flow regime and a certain dispersion when reduced to the correlation expressions [18], it could be noted that the computational results partially fall within the scatter band of the experimental data in the transitional and turbulent regime. The maximum differences between the experimental data and the best predictions of the applied turbulence models (SST model and RSM) in the turbulent region are less than 10%, which indicates that the selected numerical models are adequate for simulating thermo-hydraulic processes in the considered complex flow geometry. The obtained results are applicable for investigating flow and heat transfer in coils with rough walls of the *d type* (according to [27]), typified by transverse corrugations or closely spaced spanwise ribs with p_c/e less than 5.

The circumferential distribution of the local Nu number has also been calculated on the 9th corrugation of spiral coil segments with curvature ratio values δ_{ave}=0.033 (5th coil turn) and δ_{ave}=0.102 (12th coil turn). At selected axial location four peripheral locations were specified: location A (θ = 0°) corresponds to the outer side of the tube cross section (the furthest from the curvature center), location B (θ = 90°) corresponds to the side of the tube cross section which is directly subjected to radiant flux, location C (θ = 180°) corresponds to the inner side of the tube cross section (the closest to the curvature center) and location D (θ = 270°) which receives heat only by air convection and conduction through the tube wall. The heat flux at the inside wall of the pipe would be redistributed in relation to

the absorbed radiant heat flux at the outside wall due to the significant circumferential wall temperature variations and conductance of the wall. Since the pipe is corrugated, the circumferential distribution of Nu number was considered both at the basic (minimum) diameter of the pipe and on the corrugation crests, at the maximum diameter of the pipe.

Comparisons of experimentally and numerically obtained distributions of local Nu number at defined positions for conditions corresponding to the transitional flow regime are shown in Fig. 6, while the corresponding values for conditions at the beginning of the turbulent region and at the end of the test range are shown in Figs 7 and 8, respectively.

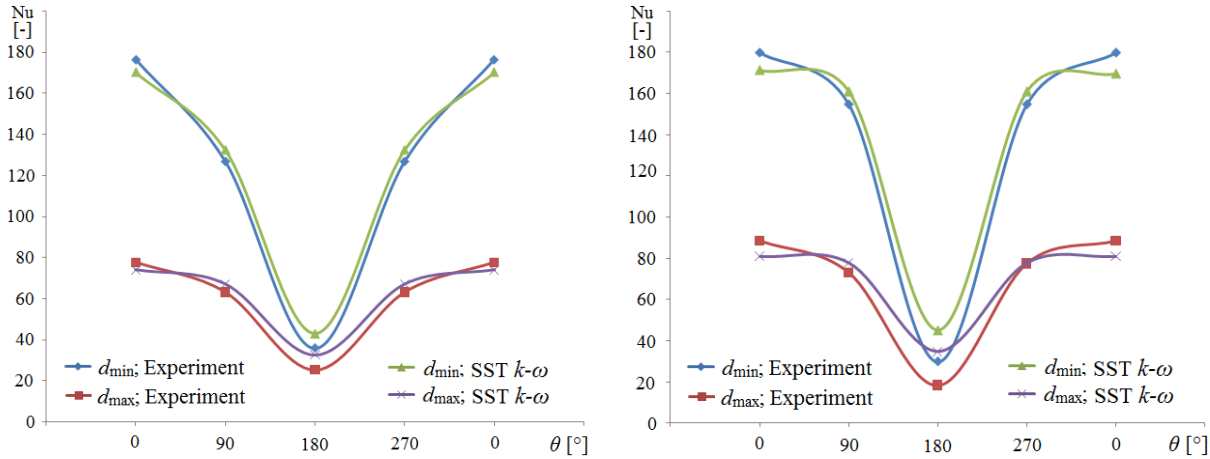

Figure 6. Circumferential distribution of Nu number: Re = 1,890, Pr=80, δ_{ave}=0.033 (left) and Re = 1,890, Pr=80, δ_{ave}=0.102 (right)

The SST k-ω turbulence model predicts relatively well the distribution of local Nu number in the transitional flow regime. It can be observed that the model slightly underpredicts values in the region of the outer wall (θ=0°) where the maximum value occurs, while it overpredicts values in the region of the inner wall (θ=180°) where the minimum value occurs. Therefore, the profiles obtained by the numerical procedure are more uniform compared to the real profiles, and the flattening effect of the numerically obtained profiles generally increases with the increase in the curvature ratio δ.

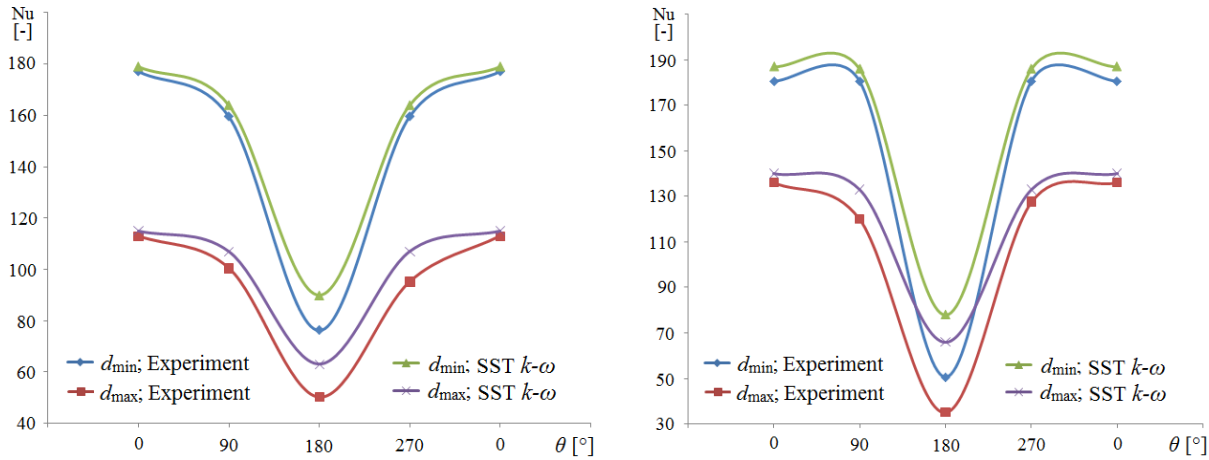

Figure 7. Circumferential distribution of Nu number: Re = 3,644, Pr=5.5, δ_{ave}=0.033 (left) and Re = 3,644, Pr=5.5, δ_{ave}=0.102 (right)

Both considered turbulence models (SST k-ω and RSM Linear Pressure-Strain) slightly overpredict the local Nu number at all positions around the circumference in the turbulent flow regime. Predictions of maximum values (θ=0°) are almost correct, while deviations occur at locations with minimum values (θ=180°), which indicates that numerical models do not adequately predict the localization of secondary flow vortices near the inner region.

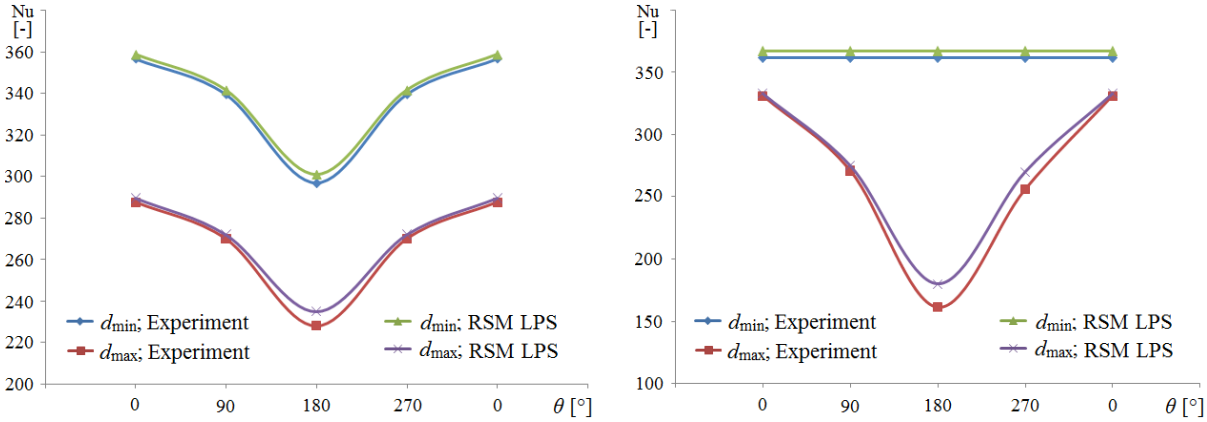

Figure 8. Circumferential distribution of Nu number: Re=15,860, Pr=5.5, δ_{ave}=0.033 (left) and Re=15,860, Pr=5.5, δ_{ave}=0.102 (right)

The differences between the experimental and numerical results are proportional to the curvature ratio δ and inversely proportional to the Re number in the turbulent range. The RSM Linear Pressure-Strain model has the ability to accurately predict complete turbulization of the flow for high values of the curvature ratio δ and Re number, when completely uniform distribution profiles of the Nu number around the circumference were obtained at the minimum diameter of the corrugated pipe (Fig. 8).

In transitional and turbulent flow regime, the predictions of numerical models are generally more accurate for locations at the minimum diameter of the corrugated pipe, while differences are noticeable for locations near the corrugation crests, at the maximum diameter of the pipe. This indicates that even the most complex RANS turbulence models do not have the ability to accurately predict the interactions between the complex flow in the basic section of the pipe and the vortex flow within the corrugations, primarily due to the boundary layer reattachment and shedding of vortex structures from the corrugations into the main flow.

4. Conclusions

A systematic numerical study of single-phase flow and heat transfer in coiled pipe with constantly varying curvature and structured roughness elements at the wall led to the synthesis of realistic numerical formulations that are consistent with the complex nature of secondary flows.

The predictions of all applied turbulence models generally overestimate the peripherally averaged Nusselt number. The use of the Realizable k-ε model with enhanced wall treatment is inadequate for predicting the heat transfer in the considered complex geometry for all flow conditions. Predictions of the applied SST k-ω and RSM Linear Pressure-Strain models agree fairly well with experimental data in the turbulent region. Both models yield uniform transition between the laminar and turbulent flow regimes, which is not in agreement with the experimental data. Predictions of both models significantly overestimate the experimentally obtained values in the laminar region, so they

can be considered inadequate for the simulation of flow and heat transfer when different flow regimes (laminar, transitional and turbulent) appear simultaneously in the spiral coil.

The SST model predictions are more accurate in the transitional and at the beginning of the turbulent region, irrespective of the curvature ratio δ. The RSM Linear Pressure-Strain model has the ability to accurately predict complete turbulization of the flow for high values of the curvature ratio δ and Re number. Characteristic for all flow regimes is that the differences between experimental data and predictions of numerical models increase with increasing curvature ratio δ, while in the turbulent region these differences decrease with increasing Re number.

The circumferential distributions of local Nu number reveal significant overpredictions of the applied turbulence models in the region of the inner wall and for locations near the corrugation crests (at the maximum diameter of the pipe). This indicates that even the most complex RANS turbulence models are unable to entirely predict the secondary flow structures, the interactions between the complex flow in the basic section of the pipe and the vortex flow within the corrugations and the boundary layer separation and reattachment.

References

[1] Ali, S., Seshadri, C., Pressure Drop in Archimedean Spiral Tubes, *Industrial and Engineering Chemistry Process Design and Development*, *10* (1971), 3, pp. 328-332

[2] Djordjević, M., *et al*., Pressure Drop and Stability of Flow in Archimedean Spiral Tube with Transverse Corrugations, *Thermal Science*, *20* (2016), 2, pp. 579-591

[3] Morton, B. R., Laminar Convection in Uniformly Heated Horizontal Pipes at Low Rayleigh Numbers, *Quarterly Journal of Mechanics and Applied Mathematics*, *12* (1959), 4, pp. 410-420

[4] Jia-dong, J., *et al*., Numerical Investigation of Flow and Heat Transfer Performances of Horizontal Spiral-Coil Pipes, *Journal of Hydrodynamic*, *28* (2016), 4, pp. 576-584

[5] Naphon, P., Study on the Heat Transfer and Flow Characteristics in a Spiral-Coil Tube, *International Communications in Heat and Mass Transfer*, *38* (2011), 1, pp. 69-74

[6] Doshmanziari, F. I., *et al*., Experimental and Numerical Study of Turbulent Fluid Flow and Heat Transfer of Al_2O_3/Water Nanofluid in a Spiral-Coil Tube, *Heat Transfer Engineering* , *38* (2017), 6, pp. 611-626

[7] Djordjević, M., *et al*., Numerical Investigation on the Convective Heat Transfer in a Spiral Coil with Radiant Heating, *Thermal Science*, *20* (2016), Suppl. 5, pp. S1215-S1226

[8] Naphon, P., *et al*., Numerical Study on the Nanofluid Flows and Temperature Behaviors in the Spirally Coiled Tubes with Helical Ribs, *Case Studies in Thermal Engineering*, *27* (2021), 101204

[9] Darzi, A., *et al*., Numerical Investigation on Thermal Performance of Coiled Tube with Helical Corrugated Wall, *International Journal of Thermal Sciences*, *161* (2021), 106759

[10] Khoshvaght-Aliabadi, M., Feizabadi, A., Compound Heat Transfer Enhancement of Helical Channel with Corrugated Wall Structure, *International Journal of Heat and Mass Transfer*, *146* (2020), 118858

[11] Zheng, L., *et al*., Numerical Investigation on Heat Transfer and Flow Characteristics in Helically Coiled Mini-Tubes Equipped with Dimples, *International Journal of Heat and Mass Transfer*, *126* (2018), Part B, pp. 544–570

[12] Zheng, Z., *et al*., Thermal Performance and Heat Transfer Reliability Analysis in Helically Corrugated Helical Tube, *International Journal of Thermal Sciences*, 183 (2023), 107849
[13] Ya-xia, L., *et al*., Fluid Flow and Heat Transfer Characteristics in Helical Tubes Cooperating with Spiral Corrugation, *Energy Procedia*, *17* (2012), pp. 791-800
[14] Cancan, Z., *et al*., Numerical Investigation of Heat Transfer and Pressure Drop in Helically Coiled Tube with Spherical Corrugation, *International Journal of Heat and Mass Transfer*, *113* (2017), pp. 332–341
[15] Zheng, Z., Yan, F., Numerical Study on Heat Transfer and Flow Resistance Characteristics of Multi-Head Twisted Spiral Tube, *Thermal Science*, *26* (2022), 2C, pp. 1883-1895
[16] Zaboli, M., *et al*., Numerical Evaluation of the Heat Transfer and Fluid Flow in a Corrugated Coil Tube With Lobe-Shaped Cross-Section and Two Types of Spiral Twisted Tape as Swirl Generator, *Journal of Thermal Analysis and Calorimetry*, *147* (2022), pp. 999–1015
[17] Di Liberto, M., Ciofalo, M., A Study of Turbulent Heat Transfer in Curved Pipes by Numerical Simulation, *International Journal of Heat and Mass Transfer*, *59* (2013), pp. 112-125
[18] Djordjević, M., *et al*., Experimental Investigation of the Convective Heat Transfer in a Spirally Coiled Corrugated Tube with Radiant Heating, *FACTA UNIVERSITATIS, Series: Mechanical Engineering*, *15* (2017), 3, pp. 495 - 506
[19] Đorđević, M., *et al*., Experimental Characterization of Heat Transfer in Coiled Corrugated Tubes, *Proceedings*, 20th Conference on Thermal Science and Engineering of Serbia - SimTerm 2022, Niš, Serbia, 2022, pp. 407-416
[20] ***, Pliable Corrugated Stainless Steel Resistant to Corrosion CSST Tubes for Plumbing, Heating Systems and Thermal Solar Plants, Eurotis S.l.r., Italy, http://www.eurotis.it
[21] ***, ANSYS FLUENT Theory Guide, Release 15.0, ANSYS Inc., USA, 2013
[22] Launder, B.E., On the Computation of Convective Heat Transfer in Complex Turbulent Flows, *Journal of Heat Transfer - Transactions of ASME*, *110* (1988), pp. 1112-1128
[23] ***, IAPWS Industrial Formulation for the Thermodynamic Properties of Water and Steam (IAPWS-IF97), The IAPWS-IF97, 2007
[24] Đorđević, M., *et al*., Experimental Investigation on the Convective Heat Transfer in a Spirally Coiled Corrugated Tube, *Proceedings*, 18th Symposium on Thermal Science and Engineering of Serbia, Soko Banja, Serbia, 2017, pp. 526-535
[25] ***, Engineering and Operating Guide for DOWFROST and DOWFROST HD Inhibited Propylene Glycol-Based Heat Transfer Fluids, Dow Chemical Company, USA, 2001
[26] Djordjević, M., *et al*., Radiant Absorption Characteristics of Corrugated Curved Tubes, *Thermal Science*, *21* (2017), pp. 2897-2906
[27] Perry, A., *et al.*, Rough Wall Turbulent Boundary Layers, *Journal of Fluid Mechanics*, *37* (1969), 2, pp. 383-413

Submitted: 20.05.2023.
Revised: 9.07.2023.
Accepted: 14.07.2023.